Analysis of Integrated Radiant Slab Heating and Cooling Systems for Residential Buildings

Benjamin Park[1] and Moncef Krarti, Ph.D., P.E.[2]

ABSTRACT: This paper presents a simulation environment developed to assess the energy use specific to integrated radiant heating and cooling systems. The developed simulation environment combines a transient finite difference solution for the two-dimensional model of an integrated radiant slab heating and cooling system with a resistance capacitance (RC) thermal network model for a multifloor building. The developed model of the integrated radiant system is able to account for thermal bridge effects on the energy performance of multifloor buildings. The predictions of the developed simulation environment are verified against those obtained from a detailed whole-building energy simulation tool under specific conditions. The developed simulation environment is then used to investigate the impact of thermal bridge effects on the performance of an integrated radiant heating and cooling system. Thermal bridging can affect significantly the energy performance of the integrated radiant systems by up to 8%. Several insulation configurations have been evaluated to assess the performance of the integrated radiant systems during both heating and cooling seasons for three U.S. locations: Chicago, IL; Golden, CO; and San Francisco, CA. A combination of horizontal and edge insulations is the most effective regardless of the building location. The most effective insulation configuration achieves up to 30% in heating energy savings and 35% in cooling energy savings compared with the building with no insulation. **DOI: 10.1061/(ASCE)AE.1943-5568.0000189.**

Introduction

A radiant heating and cooling system transfers heat through temperature-controlled surfaces to or from an indoor space, and its enclosure surfaces by thermal radiation and natural convection. Generally, most of the heat transfer between panel surface and the space occurs through thermal radiation. Panel heating and cooling systems can be used to maintain thermal comfort in a wide range of building types including residences, office buildings, and industrial applications.

Radiant heating and cooling systems have become popular because of their potential for energy savings as well as better thermal comfort (uniform cooling and heating distribution). Radiant panel systems have several advantages. Hydronic panel systems may be connected in series increasing exergetic efficiency. Indoor air and mean radiant temperatures can be controlled with the radiant panels, minimizing air motion within a space. Therefore, thermal comfort may be better maintained with radiant systems than with conventional air-conditioning systems. Moreover, radiant panel systems have relatively low initial cost compared with air-conditioning systems. They also require less space for mechanical equipment and control devices. This feature is especially valuable in hospital patient rooms, offices, and other applications where space is at a premium. Moreover, in-floor heating creates inhospitable living conditions for house dust mites compared with other heating systems. With radiant systems, noise associated with fan-coil or induction units is eliminated. In addition, peak loads are reduced as a result of thermal storage capabilities of the thermal mass of the building, which can be enhanced by passing a hot or a chilled fluid through pathways into the structure.

Ho et al. (1995) developed detailed numerical models for radiant panels that rely on a two-dimensional (2D) formulation scheme. Stetiu (1998) concluded that radiant systems can save up to 30% of the energy consumption and 27% of the peak demand for U.S. office buildings. Zhang (2001) developed a one-dimensional (1D) model to simulate the dynamic behavior of the under-floor heating system for several control strategies. Laouadi (2004) developed a slab floor model combining a 1D numerical model with a 2D analytical model in exploring the temperature distribution between the tubes arranged in the serpentine tubing configuration. Watson and Chapman (2002) reported that radiant systems can benefit from building thermal mass to shift the peak hour and enhance a thermal comfort in the space. Weitzman et al. (2005) developed detailed numerical models of radiant systems that rely on a 2D formulation scheme. Theoretical or experimental results show that radiant ceiling panels can achieve energy savings up to 30% compared with conventional air systems (Zhang 2001). Several factors, such as design capacities, temperature settings, and locations of the radiant panels, affect the energy efficiency of the systems and the thermal comfort of the occupants. Properly designed systems can produce long-term energy savings of up to 30% (Conroy and Mumma 2001; Mumma 2001). In addition, several studies have been performed using transient numerical modeling of radiant slab floor systems to evaluate their thermal performance for a specific set of control strategies under transient conditions.

However, most of these studies are based on simplified models of the radiant heating or cooling systems without considering integrated systems that can be used for both heating and cooling. Moreover, the existing models neglect the impact of thermal bridging effects on the performance of radiant systems. Typically, a radiant floor heating system's floor surface temperature is higher than

[1]Doctoral Candidate, Dept. of Civil, Environmental and Architectural Engineering, Univ. of Colorado Boulder, UCB 428, Boulder, CO 80309.

[2]Professor, Dept. of Civil, Environmental and Architectural Engineering, Univ. of Colorado Boulder, UCB 428, Boulder, CO 80309 (corresponding author). E-mail: krarti@colorado.edu

Note. This manuscript was submitted on February 4, 2015; approved on July 27, 2015; published online on December 3, 2015. Discussion period open until May 3, 2016; separate discussions must be submitted for individual papers. This paper is part of the ***Journal of Architectural Engineering***, © ASCE, ISSN 1076-0431.

when an air-based system conditions the building. A radiant cooling system lowers the surface temperature to achieve the desired mean air temperature. Therefore, the thermal bridge effect becomes important for evaluating the thermal performance and the energy performance of integrated radiant heating floor and cooling ceiling systems. In this paper, a 2D numerical model is combined with a resistance capacitance (RC) network to develop a simulation environment for integrated radiant heating and cooling systems. The simulation environment is then used to evaluate the impact of the thermal bridging effects on the performance of integrated radiant heating and cooling systems.

Simulation Environment Development

FDM Model

A control volume approach and pure implicit finite difference technique is used to solve the 2D heat conduction equation with heat sources represented by Eq. (1). The 2D numerical solutions for radiant floor heating and cooling systems are developed by adding heat generation and extraction sources using embedded hot and chilled water pipes within the floor slab. (Çengel et al. 2001; Patankar, 1980)

$$K\frac{\partial^2 T}{\partial x^2}+K\frac{\partial^2 T}{\partial y^2}+q=\rho c_p\frac{\partial T}{\partial t} \tag{1}$$

The actual heat transfer between the building element (i.e., slab) and the hydronic radiant system is related to the temperature of the slab at the source location and the water inlet and outlet temperatures. It is assumed that the fluid in the tubing is water. In addition, another assumption is that the thermal properties of the water do not vary significantly over the length of the tubing. The hydronic radiant system embedded in the slab is thought of as a heat exchanger. The effectiveness number of transfer units (ε-NTU) heat exchanger algorithm is used to define the heat flux to the slab from the heat sources, because the water outlet temperature is unknown. (Uiuc 2005; Kreith and Bohn 2001) The calculated heat flux can be thought of as a heat generation and then used to heat balance calculations using the finite difference method.

In accordance with a heat balance on a hydronic loop and the second law of thermodynamics, the effectiveness of the heat exchanger, ε, is defined as the ratio of the actual energy transfer to the maximum amount of energy transfer

$$\varepsilon\equiv\frac{q}{q_{\max}}=\frac{(\dot{m}c_p)_{\text{water}}(T_{w,\text{in}}-T_{w,\text{out}})}{(\dot{m}c_p)_{\text{water}}(T_{w,\text{in}}-T_s)} \tag{2}$$

When one fluid is stationary for a heat exchanger, the effectiveness can be related to the NTU. (Bergman et al. 2006)

$$\varepsilon=1-e^{-\text{NTU}}\equiv 1-e^{-\frac{h_w(\pi DL)}{(\dot{m}cp)_{\text{water}}}} \tag{3}$$

The convection coefficient, h, can be calculated from the internal flow correlations, which are related to the Nusselt, Reynolds, and Prandtl numbers. The convective coefficient of water can be determined using the Dittus–Boelter correlation.

The heat generation and extraction sources within the floor slab can be calculated by solving Eq. (2). The calculated heat generation and extraction source can be added at each node where the heat source is located, as shown in Eq. (1) (Patankar 1980).

A nonuniform geometric discretization scheme is applied to reduce the computational efforts and the memory requirements significantly. In particular, as shown in Fig. 1, the discretization grid is very fine near the surface boundary and interaction between two different materials and near the boundary of heat sources. The grid is gradually expanded in the area where relatively smaller temperature changes are expected.

Fig. 2 illustrates the schematic of the simulation environment using both a RC thermal network model for two thermal zones of a two-story building and a 2D finite difference method (FDM) model for the integrated radiant slab/ceiling system. The FDM technique is used to solve Eq. (1) within the building envelope components, which include an embedded heat source (i.e., floor and ceiling). In contrast, a RC network (3R2C) is used to estimate heating and cooling loads with thermal zones. The developed simulation environment adopts the simplified window model that accepts U-factor and solar heat gain coefficient (SHGC) values. Simplified solar distribution on interior surfaces is also considered in the developed RC network model. This distribution method assumes that all transmitted direct radiation is incident on the floor and absorbed depending on the floor solar absorptance. The reflected portion is assumed to be diffuse and is uniformly absorbed by all surfaces. All transmitted diffuse radiation is uniformly absorbed by all of the zone surfaces. Both the floor and ceiling surface temperatures are obtained using the FDM solution, whereas the radiative and convective heat transfer exchanges between zone surfaces including the walls, the floor, and the ceiling are accounted for using a RC network model combined with indoor air heat balance. Fig. 2 also illustrates the relationship between the heat transfer mechanisms for various surfaces using the developed simulation environment, which combines a RC network and a FDM numerical solution (FDMRC) of zones equipped with radiant slab systems.

In the developed simulation environment, algorithms have been included to control the zone indoor air temperature to be within predefined setpoint temperatures and throttling ranges. In particular, variable flow control strategies are considered to modulate the operation of the integrated radiant heating and cooling slab systems. Specifically, the radiant systems can vary the water flow rate from zero up to a specified maximum water flow rate. The flow rate is varied linearly on an hourly basis; meanwhile, the inlet water temperature remains constant (Strand and Pedersen 1997). In the analysis presented in this study, the indoor mean air temperature is used as a thermal load indicator to control the water flow rate. However, other thermal comfort indicators, such as radiant mean temperature, can be used to control the water flow rate. Fig. 3 illustrates variable water flow rate control strategies used for the integrated radiant slab systems and implemented in the simulation environment.

RC Network Model

A 3R2C thermal network has been widely used to simulate the thermal performance of the building envelope. Wang and Xu (2006) concluded that the frequency characteristics of the 3R2C model should approach the theoretical frequency characteristics of the building envelope as closely as possible. The accuracy of various RC thermal network models (2R1C, 3R2C, and 6R4C) was evaluated by comparing the measured average room air temperature in the alpine lodging building in the Swiss Alps (Fux et al. 2014). The authors concluded that the 3R2C thermal network model can accurately predict the room air temperature (Fux et al. 2014). The 3R2C models have been successfully used to simulate the building envelopes for transient building load prediction (Braun and Chaturvedi 2002; Seem 1987).

Envelope	Boundary conditions	Enlarged non-uniform grid generation at wall-slab joint
Exterior Wall	Exposed to outdoor air Exposed to solar	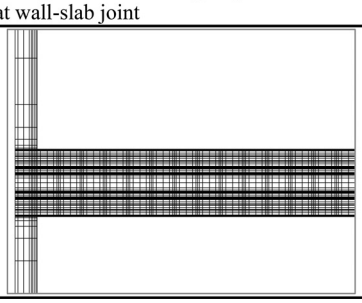
Exterior Roof	Exposed to outdoor air Exposed to solar	
Exterior Floor	Ground contact with constant temperature (18°C)	

Fig. 1. Summary of boundary conditions for exterior envelope and example of nonuniform grid generation for 2D FDM numerical solution

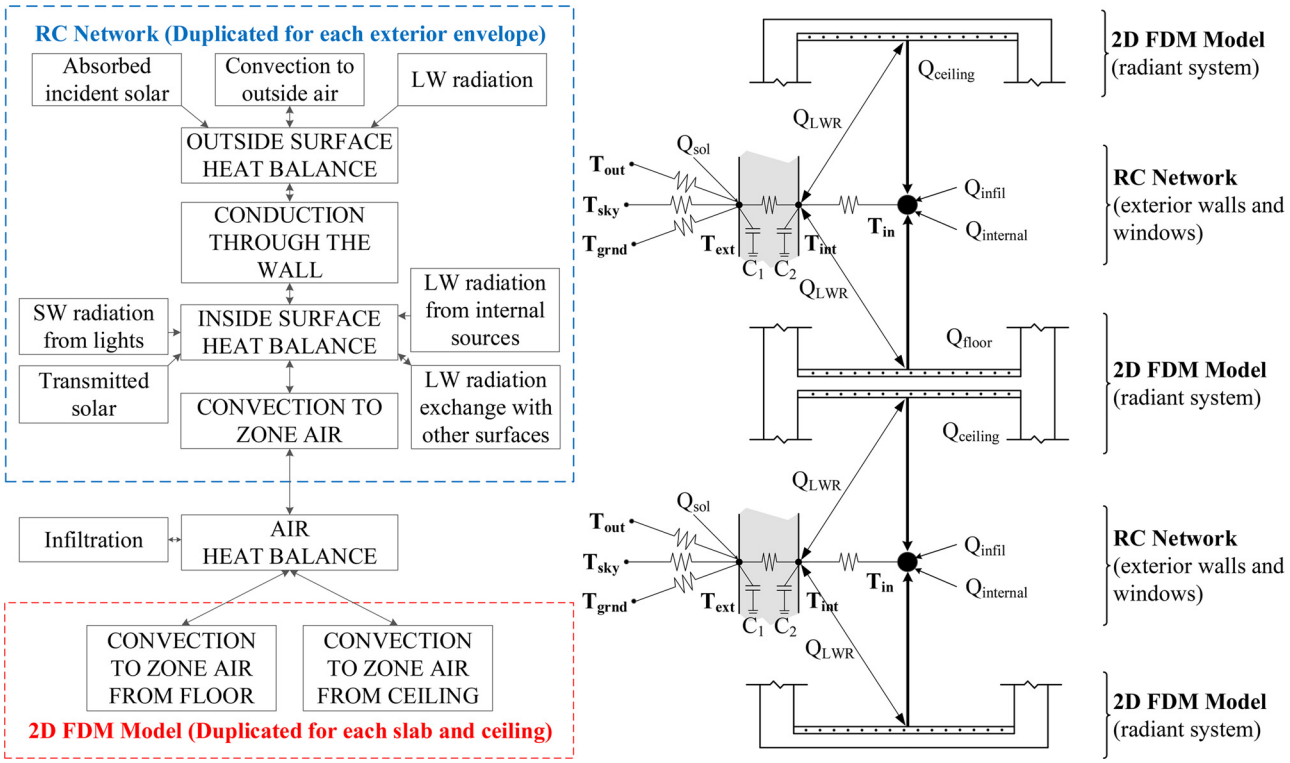

Fig. 2. Schematic of heat balance calculation procedure of the developed 2D FDMRC simulation environment

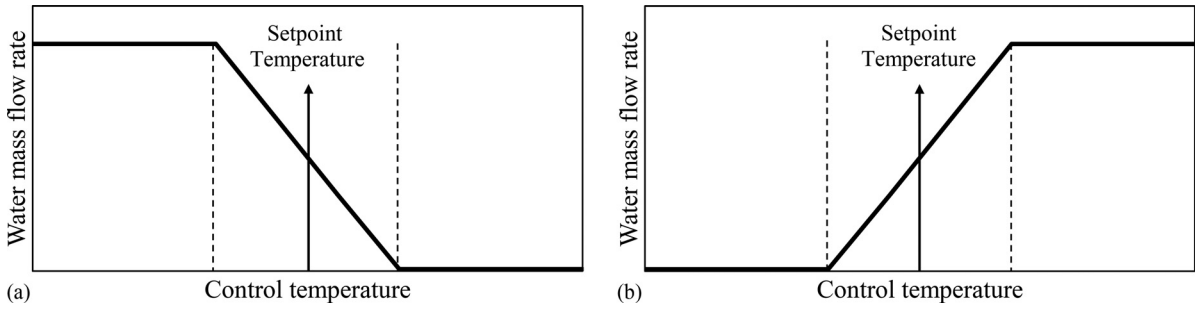

Fig. 3. Variable flow control schemes: (a) heating mode; (b) cooling mode

Fig. 4 depicts a 3R2C thermal network of an exterior wall that is used in the simulation environment. All the resistances and capacitances are assumed to be time invariant. Convection and long-wave radiation exchanges along both sides and short-wave solar radiation incidence at the outside surface of the exterior wall affect the wall temperature as follows:

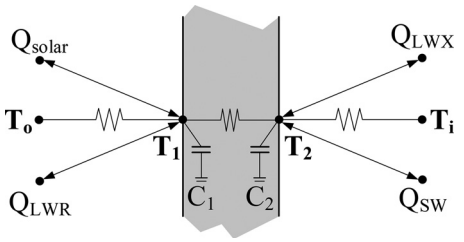

Fig. 4. Schematic of the RC thermal network model of the exterior wall

$$C_1 \frac{dT_1}{dt} = \frac{T_2 - T_1}{R} + h_o A(T_{\text{out}} - T_1) + Q_{\text{LWR}} + Q_{\text{SOLAR}}$$

$$C_2 \frac{dT_2}{dt} = \frac{T_1 - T_2}{R} + h_i A(T_{\text{zone}} - T_2) + Q_{\text{LWX}} + Q_{\text{SW}}$$

Indoor Air Heat Balance

The fundamental feature of the developed simulation environment is the indoor air heat balance model. This model combines the FDM slab model and a RC thermal network. Eq. (4) expresses the indoor air heat balance and includes convective heat transfer from building envelope surfaces and internal loads (ASHRAE 2005). Sensible load caused by air ventilation is neglected

$$q_{\text{conv,FDM}} + q_{\text{conv,RC}} + q_{\text{CE}} + q_{\text{IV}} + q_{\text{sys}} = 0 \tag{4}$$

Convective Coefficients

Interior convective heat flux along interior surfaces is a function of the surface temperature and the air-layer temperature directly in contact with the surfaces. Various convective heat transfer coefficient correlations have been developed and reported in the literature. For the simulation environment, a correlation to estimate heat transfer coefficient for natural convection along vertical walls is adopted (ASHRAE 2005)

$$h = 1.31|\Delta T|^{\frac{1}{3}} \tag{5}$$

A comprehensive convective algorithm developed by Walton (1983) is adopted in the FDMRC simulation environment for interior convective coefficient for any surface related to the radiant slab system. Specifically, the convective coefficients along the surfaces depend on the direction of heat flow and the buoyancy as shown by Eqs. (6) and (7), respectively.

$$h = \frac{9.482|\Delta T|^{\frac{1}{3}}}{7.283 - |\cos \Sigma|} \tag{6}$$

$$h = \frac{1.810|\Delta T|^{\frac{1}{3}}}{1.382 - |\cos \Sigma|} \tag{7}$$

The *DOE-2* convection model (*DOE.1E-053*) is adopted for the FDMRC to calculate exterior convective coefficient and combines the *MoWiTT* and *BLAST* (DOE 2012) detailed convection algorithms. The convection coefficient for very smooth surfaces is calculated by Eq. (8)

Table 1. *MoWiTT* Coefficients (Data from Yazdanian and Klems 1994)

Wind direction	Ct (W/m^2 K$^{4/3}$)	a [W/m^2 K(m/s)^b]	b (–)
Windward	0.84	3.26	0.89
Leeward	0.84	3.55	0.617

$$h_{c,\text{glass}} = \sqrt{h_n^2 + (aV_z^b)^2} \tag{8}$$

where h_n is calculated using Eqs. (6) and (7); and the constants a and b are given in Table 1 (Yazdanian and Klems 1994). For rough surfaces, the convection coefficient is modified according to Eq. (9)

$$h_o = h_n + R_f(h_{c,\text{glass}} - h_n) \tag{9}$$

For radiant slab systems, air is typically circulated within the embedded pipes. Therefore, the convection heat transfer coefficient of the fluid circulated in the pipes can be determined using the Dittus–Boelter correlation (Holman 1997)

$$h_w = \frac{Nu \cdot K_w}{D} \tag{10}$$

where $Nu = 3.36$ if (Re < 2300); and $Nu = 0.023\text{Pr}^n\text{Re}^{0.8}$ else with $n = 0.4$ for heating and $n = 0.3$ for cooling.

Internal Radiation Heat Exchange

Two surfaces at different temperatures exchange heat energy by thermal radiation. The FDMRC simulation environment uses a gray interchange model to account for thermal radiation heat exchange between interior surfaces. In particular, the radiosity concept developed by Hottel and Sarofim (1967) is used by the simulation environment. The net radiative heat transfer at a surface can be determined by Eq. (11)

$$Q_i = \frac{A_i \varepsilon_i}{1 - \varepsilon_i}(\sigma T_i^4 - J_i) \tag{11}$$

where the radiosity, J, is the sum of the gray body radiation occurred by temperature T; and the incident radiation, H, as shown in Eq. (12)

$$J = \varepsilon \sigma T^4 + (1 - \varepsilon)H \tag{12}$$

The incident radiation, H, is normally unknown. If a certain surface i is hit by radiation from another surface j, the radiation heat energy incident on surface i can be described as Eq. (13), where F_{ji} is the view factor from surface j to i (Çengel et al. 2001)

$$H_i = \frac{\sum_{j=1}^{N} F_{ji} A_j J_i}{A_i} \tag{13}$$

Window Heat Balance Model

Arasteh et al. (2010) outlined a procedure to determine window properties, such as glass-to-glass resistance, thickness, thermal conductivity, transmittance, and glazing reflectance by using only U-factor and SHGC values. The FDMRC simulation environment uses the simplified window model–based U-factor and SHGC values to determine the properties of the window glazing.

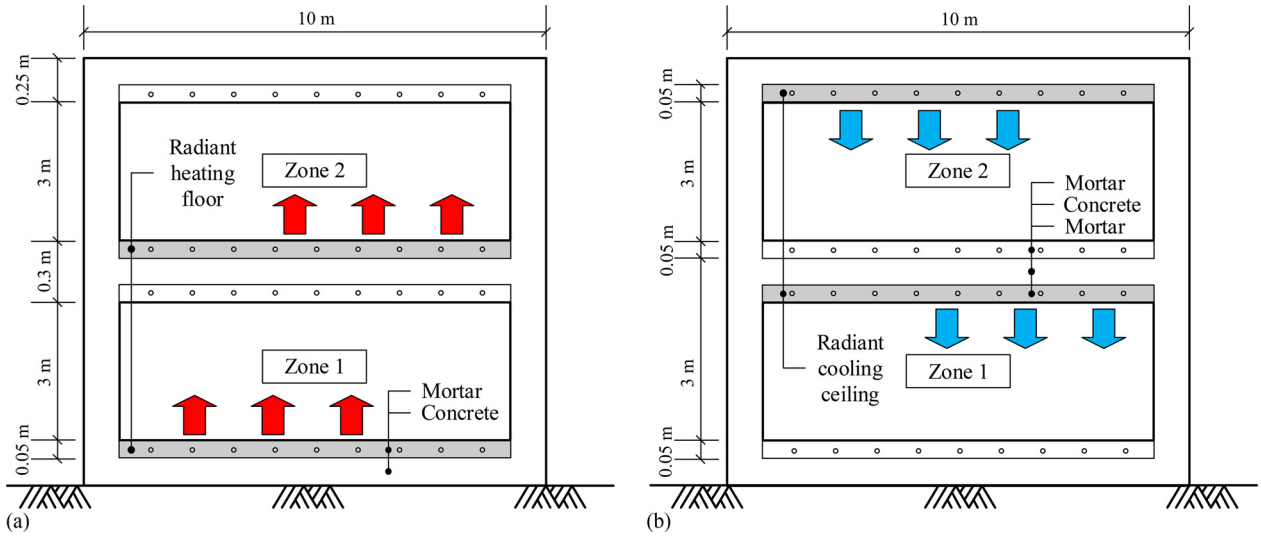

Fig. 5. A section view of the building slab and exterior walls for two thermal zones used for the verification analysis: (a) radiant heating floor; (b) radiant cooling ceiling

Eq. (14) expresses the heat balance for a single-glazed window. Few assumptions are made in deriving the window heat balance equations. It is assumed that the glass is thin enough so that heat storage within the glazing is neglected, and that the short-wave radiation absorbed is equally distributed to the two faces of the window glazing

$$E_o\varepsilon_{\text{win}} - \varepsilon_{\text{win}}T_{\text{win},o}^4 + k_{\text{win}}(T_{\text{win},i} - T_{\text{win},o}) + h_o(T_o - T_{\text{win},o}) + S_{\text{win},o} = 0$$

$$E_i\varepsilon_{\text{win}} - \varepsilon_{\text{win}}T_{\text{win},i}^4 + k_{\text{win}}(T_{\text{win},i} - T_{\text{win},o}) + h_i(T_i - T_{\text{win},i}) + S_{\text{win},i} = 0 \quad (14)$$

Apart from window heat balance, it is also necessary to consider the interior surfaces that absorb solar radiation, which has been transmitted through the fenestration. The developed simulation environment uses a simplified interior solar distribution model that assumes all transmitted direct radiation is incident on the floor and absorbed as a function of the floor solar absorptance. The reflected portion is assumed to be diffuse and is uniformly absorbed by all surfaces. All transmitted diffuse radiation is uniformly absorbed by all of the zone surfaces, including the floor surface. Eqs. (15) and (16) provide expressions for the absorbed solar radiation for interior surfaces and floor, respectively

$$q_{\text{solar},in,j,\theta} = \frac{\sum \dot{q}_{\text{TSHG,diffuse}} + (1 - \alpha_{\text{floor}})\sum \dot{q}_{\text{TSHG,direct}}}{\sum_{j=1}^{N} A_j} \quad (15)$$

$$q_{\text{solar,in,floor},\theta} = \frac{\sum \dot{q}_{\text{TSHG,diffuse}} + (1 - \alpha_{\text{floor}})\sum \dot{q}_{\text{TSHG,direct}}}{\sum_{j=1}^{N} A_j} + \frac{\alpha_{\text{floor}}\sum \dot{q}_{\text{TSHG,direct}}}{A_{\text{floor}}} \quad (16)$$

Table 2. Basic Features of Building Envelope and the Integrated Radiant Slab System Used for Validation Analysis

Building component	Parameter	Value
Slab (floor)	U-value	5.94 W/m^2 K (with no insulation)
Roof (ceiling)	U-value	5.94 W/m^2 K (with no insulation)
Exterior wall	U-value	0.45 W/m^2 K
Fenestration	U-value	2.96 W/m^2 K
	SHGC	0.385
	Window-to-wall ratio	34.6% (only east and west)
Radiant system	Pipe diameter	0.015 m
	Pipe length	480 m
	Control type	Variable flow rate
	Maximum water flow rate	0.5 kg/s
	Throttling range	±1°C
	Setpoint	
	Heating	19°C
	Cooling	25°C
	Water inlet temperature	
	Heating	40°C
	Cooling	15°C

Model Verification

Predictions of mean air temperature and radiant energy consumption obtained from EnergyPlus are used to verify results obtained from the FDMRC simulation environment. The existing radiant system module of EnergyPlus was validated using results from an experimental testing analysis (Ghatti 2003). Specifically, the cooling energy use and the indoor operative temperatures predicted by the EnergyPlus module were found to agree well with measured data obtained for a residential building in Carefree, AZ. Fig. 5 presents a building section with two thermal zones considered in the verification analysis using both EnergyPlus and the FDMRC simulation environment. The verification analysis is conducted using weather data for Golden, CO, obtained from a TMY3 weather file for specific days representative of winter and summer conditions.

For radiant systems, it is recommended that room temperature is set between 18 and 22°C and supply hot water temperature ranges from 35 to 60°C (Watson and Chapman 2002; ASHRAE 2008). In a stand-alone panel cooling system, dehumidification and panel surface condensation may be a significant concern under specific operating conditions. In particular, preventing condensation problems can affect the selection of the cooling capacity of a radiant system. The surface temperature should not be equal or below the dew point temperature within the space. Some standards suggest a limit for the indoor relative humidity to be 60% or 70%. An air temperature of 26°C would mean a dew point between 17 and 20°C (Olesen 2008). There is, however, evidence that suggests decreasing the surface temperature to below the dew point temperature for a short period of time may not cause condensation issues (Mumma 2002). As a general rule of thumb, it is recommended to maintain the slab surface higher than 20°C. A water temperature of 16 ± 1°C is recommended for radiant cooling systems to reduce the risk of condensation. Also, it is recommended to use an additional system, such as a dehumidifier, to reduce the indoor relative humidity and allow for increased cooling capacity.

These guidelines are considered to define the two-zone building model used for the verification analysis. Specifically, the zone model includes the radiant heating floor system and the radiant cooling ceiling system embedded in a concrete slab. The length of the radiant floor is 10 m. The thickness of the exterior walls is 0.15 m. The pipe pitch size is 0.3 m. The length of the embedded pipes is assumed to be 480 m, and its diameter is 0.015 m. The total area of radiant slab heating and cooling panels is 100 m^2. Heating and cooling setpoint temperatures are assumed to be 19 and 25°C, respectively, for 24 h/day. All outside surfaces of the building envelope except for the lower

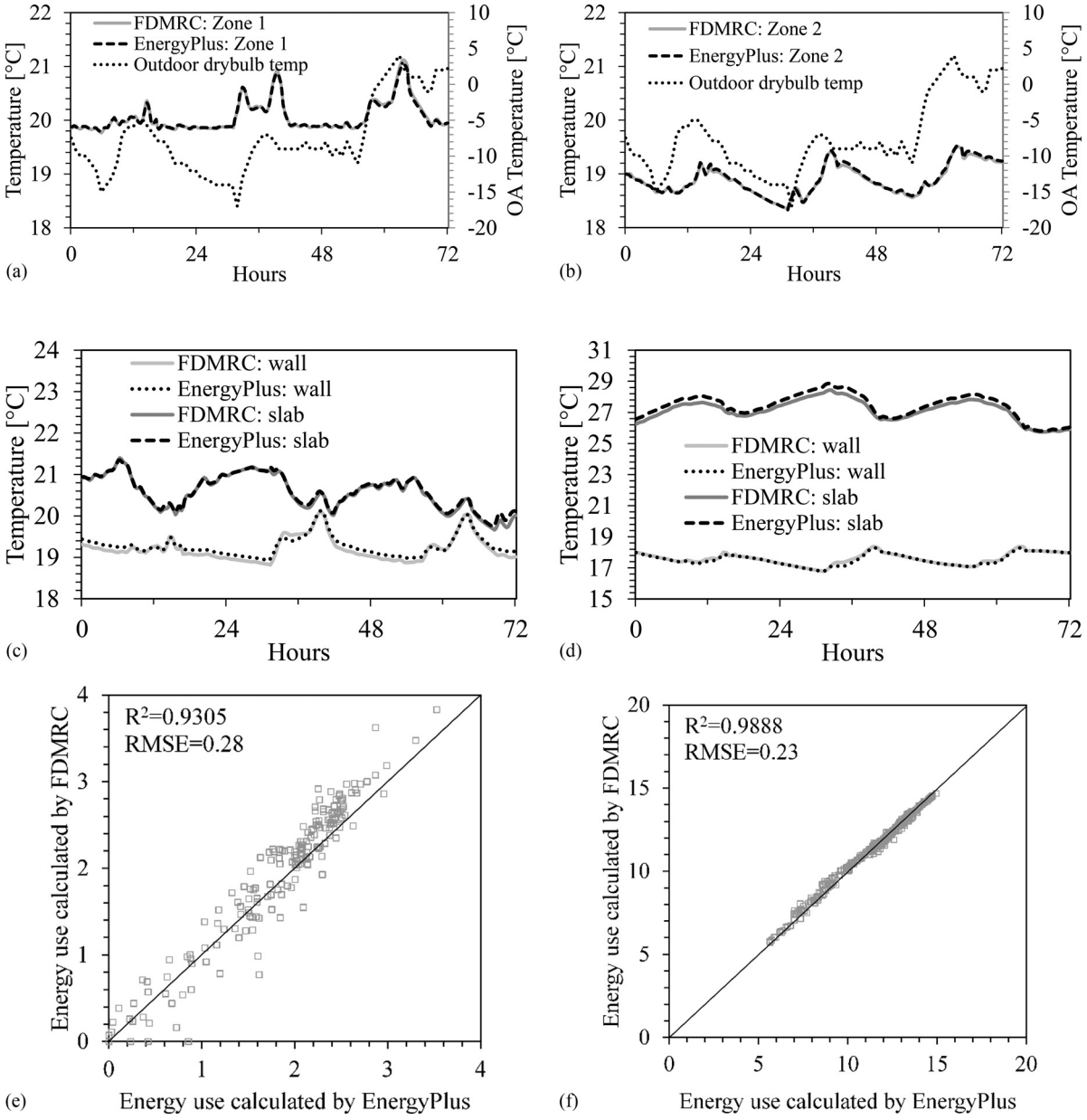

Fig. 6. Comparison of mean air temperatures, inside surface temperatures, and heating energy use and prediction root mean square error (RMSE) for Zones 1 and 2 obtained from EnergyPlus and the developed 1D FDMRC from January 2 to January 4: (a) mean air temperature for Zone 1; (b) mean air temperature for Zone 2; (c) surface temperatures for Zone 1; (d) surface temperatures for Zone 2; (e) heating energy use for Zone 1; (f) heating energy use for Zone 2

zone floor are exposed to outdoor air. The floor of the lower zone is assumed to be in contact with the ground set with a constant temperature (18°C). Table 2 provides a summary of the building model features and the control parameters for the integrated radiant floor heating system and the radiant cooling ceiling system.

Using the developed simulation environment, the radiant heating energy consumption and radiant cooling energy are calculated for each time step using Eq. (15)

$$E_{\text{heating}} = \dot{m}_h c_{p,h}(T_{h,w,\text{in}} - T_{h,w,\text{out}})$$

$$E_{\text{cooling}} = \dot{m}_c c_{p,c}(T_{c,w,\text{out}} - T_{c,w,\text{in}}) \quad (17)$$

As part of the verification analysis, the predictions of mean air temperature and radiant system energy consumption for the lower zone (Zone 1) and the upper zone (Zone 2) obtained from the developed simulation environment, which combines a RC network and the 1D FDM numerical solution (1D FDMRC) during heating season (January 2–4) and cooling season (August 3–5), are verified against results obtained from EnergyPlus. It should be noted that the 1D FDM solution is obtained by setting adiabatic boundary conditions at the slab and wall joint in the model of Fig. 5. Fig. 6 shows a comparative analysis of mean air temperature, surface temperatures, and heating energy consumption of the radiant system for each zone obtained from the 1D FDMRC and EnergyPlus. As shown in Fig. 6, the mean air temperature of the upper zone swings more than that of the lower zone, because the ceiling in the upper zone is exposed to outdoor conditions, whereas the lower zone is in contact with the ground medium set at a constant temperature. Moreover, the heating thermal load of the upper zone is greater than that of the lower zone. By comparing the mean air temperatures and radiant heating energy consumption during the heating season, the results of both simulation tools showed good agreement with similar patterns under the same operation and environment conditions.

Similarly, time variations of outdoor temperature, zone mean air temperatures, and radiant cooling energy usage for each zone

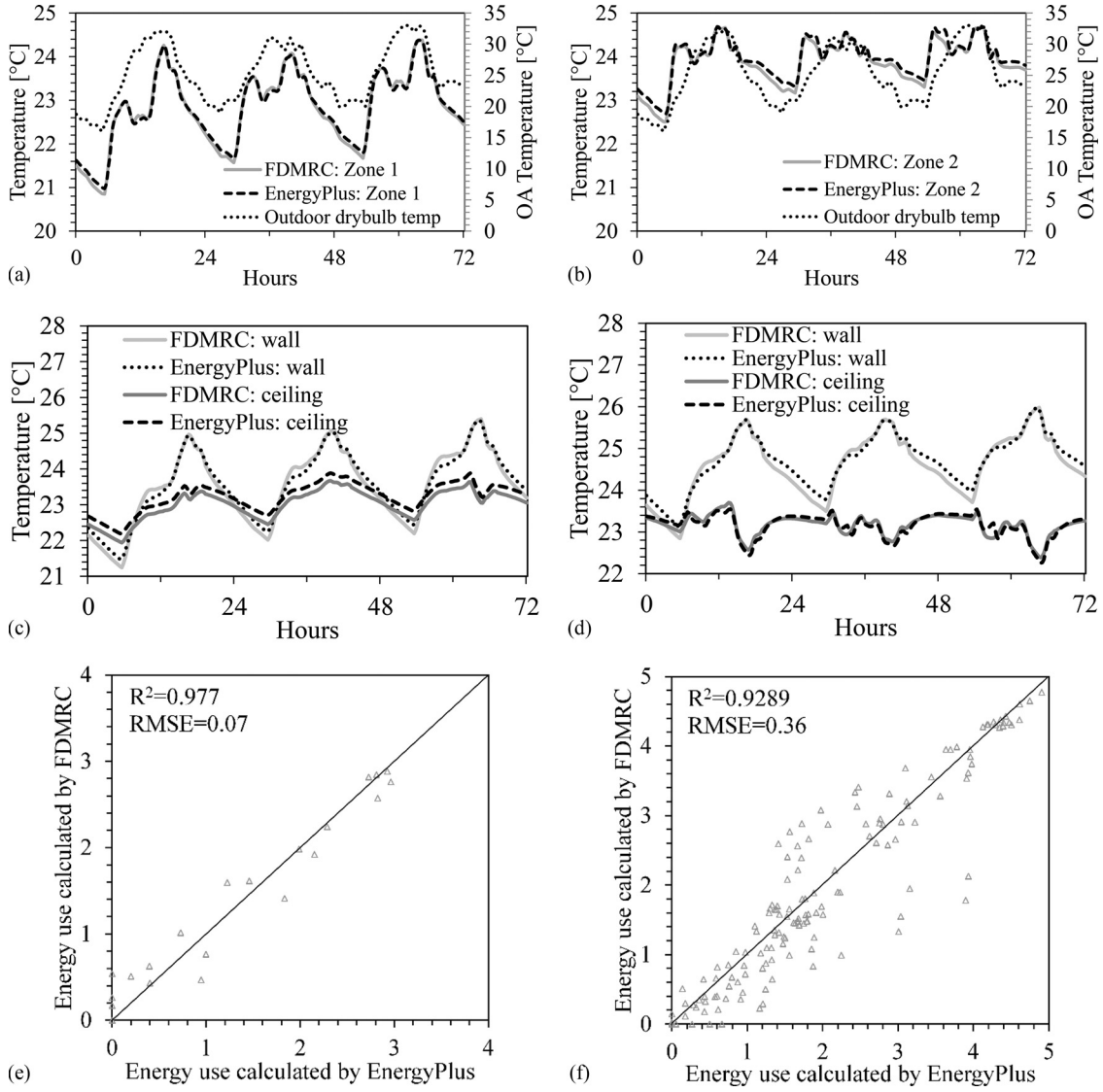

Fig. 7. Comparison of mean air temperatures, inside surface temperatures, and heating energy use and prediction root mean square error (RMSE) for Zones 1 and 2 obtained from EnergyPlus and the developed 1D FDMRC from August 3–5th: (a) mean air temperature for Zone 1; (b) mean air temperature for Zone 2; (c) surface temperatures for Zone 1; (d) surface temperatures for Zone 2; (e) heating energy use for Zone 1; (f) heating energy use for Zone 2

predicted by the two simulation tools during three summer days are depicted in Fig. 7. The predictions of mean air temperature and radiant cooling energy consumption obtained from the 1D FDMRC agreed well with the results of EnergyPlus.

Table 3. Characteristics of Building Envelope, Internal Loads, and the Integrated Radiant Slab System

Building component	Parameter	Value
Slab (floor)	U-value	5.94 W/m^2 K (with no insulation)
Roof (ceiling)	U-value	5.94 W/m^2 K (with no insulation)
Exterior wall	U-value	0.45 W/m^2 K
Fenestration	U-value	2.96 W/m^2 K
	SHGC	0.385
	Window-to-wall ratio	34.6% (only east and west)
Internal load	Occupancy	Number of people: 2 (each zone)
	Lighting	Power density: 0.8 W/m^2
	Infiltration	0.082 m^3/s
Radiant system	Pipe diameter	0.015 m
	Pipe length	273 m
	Control	Variable flow rate
	Maximum water flow rate	0.5 kg/s
	Throttling range	±1°C
	Setpoint	
	Heating	19°C
	Cooling	25°C
	Water inlet temperature	
	Heating	40°C
	Cooling	15°C

Thermal Bridging Effect Analysis

In this section, the effect of thermal bridging caused by the floor slab-wall joint is investigated by estimating the total radiant heating and cooling energy consumption of the integrated radiant heating floor and the radiant cooling ceiling system operated with a variable flow control strategy. To estimate the impact of thermal bridging effects, predictions of the developed simulation environment, combining a RC network model and the 2D FDM numerical solution (2D FDMRC), are compared with those obtained from the 1D FDMRC. Specifically, the 1D FDMRC, which agrees well with EnergyPlus, does not account for thermal bridging and has no heat losses through the slab edges. In contrast, the 2D FDMRC accounts for the thermal bridging between the floor slab-wall joint and has heat transfer through the slab edges. Table 3 summarizes the characteristics of the building envelope, the internal loads, and the integrated radiant slab system considered in the simulation analysis.

Figs. 8 and 9 present the time variations of zone mean air temperature and radiant energy consumption predicted by the developed simulation environment using both the 1D and 2D numerical solutions during heating and cooling seasons, respectively. Based on the results, the time variations of mean air temperatures computed by the 1D and 2D FDMRCs are almost identical, because the variable flow control strategy is maintaining the same desired indoor temperature with each thermal zone. However, there is a substantial difference in heating energy use and cooling energy use predicted using the two numerical solutions. As summarized in Table 4, the uninsulated radiant system, without accounting for the thermal bridging effects (i.e., estimated with the 1D FDMRC), consumes 2,981 MJ of heating source energy; meanwhile, the same radiant system considering the thermal bridging effects (i.e., estimated with the 2D FDMRC) consumes 3,168 MJ of heating energy in the heating season (i.e., a 6% difference). Moreover, the uninsulated radiant system, without accounting for the thermal bridging

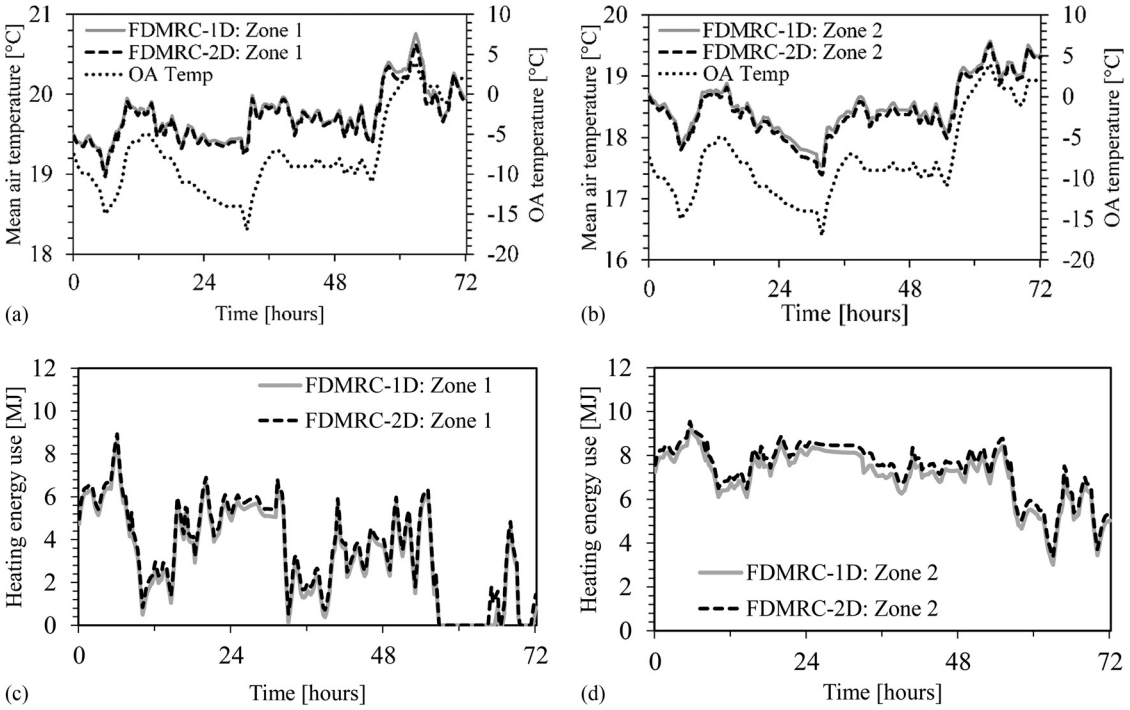

Fig. 8. Comparison of mean air temperatures and heating energy use for Zones 1 and 2 obtained from the 1D and 2D FDMRC from January 2 to January 4 in Golden, CO: (a) mean air temperature for Zone 1; (b) mean air temperature for Zone 2; (c) heating energy use for Zone 1; (d) heating energy use for Zone 2

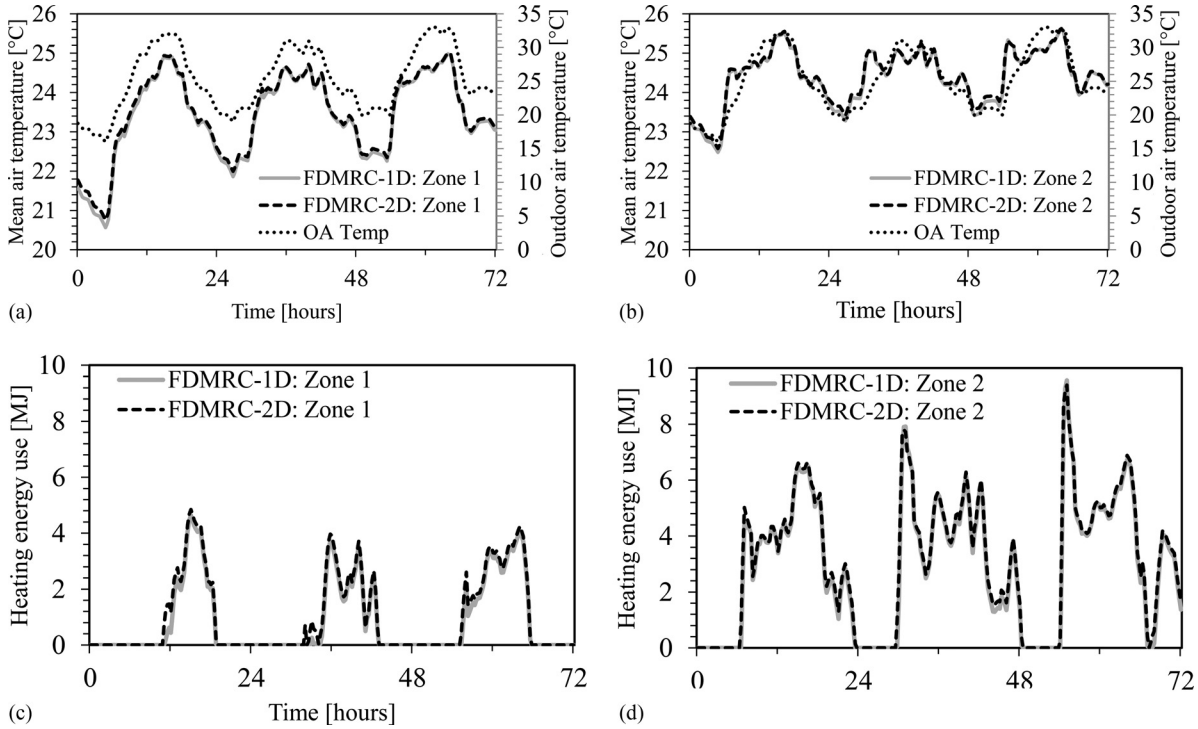

Fig. 9. Comparison of mean air temperatures and cooling energy use for Zones 1 and 2 obtained from the 1D and 2D FDMRC from August 3 to August 5 in Golden, CO: (a) mean air temperature for Zone 1; (b) mean air temperature for Zone 2; (c) cooling energy use for Zone 1; (d) cooling energy use for Zone 2

Table 4. Summary of Energy Consumption by the Radiant System and Estimation of Thermal Bridging Effects during Heating Season (January 2–4) and Cooling Season (August 3–5) for 8-m-Wide Slab in Golden, CO

	Heating energy use (MJ)			Cooling energy use (MJ)		
Category	Zone 1	Zone 2	Total	Zone 1	Zone 2	Total
1D FDMRC	944	2,037	2,981	258	840	1,098
2D FDMRC	1,023	2,145	3,168	289	895	1,184
Absolute difference	79	108	188	31	54	85
% Difference	8%	5%	6%	12%	6%	7%

effects (i.e., computed using the 1D FDMRC), consumes 1,098 MJ of cooling source energy; meanwhile, the same radiant system, considering the thermal bridging effects (i.e., computed using the 2D FDMRC), consumes 1,184 MJ of cooling energy in the cooling season (i.e., a 7% difference). Thus, the 1D FDMRC neglects the additional heating and cooling thermal loads caused by thermal bridging effects at the slab-wall joint.

To assess the impact of adding insulation on the thermal bridging effects for the integrated heating and cooling radiant system, energy consumption obtained from the 2D FDMRC with the vertical insulation placement with various R values are compared with energy consumption of the radiant system predicted by the 1D FDMRC. Fig. 10 illustrates the energy performance of the integrated radiant system as a function of the R value of the vertical insulation during both winter and summer seasons for various slab widths. As the R value of the vertical insulation increases, energy consumption obtained from the 2D FDMRC becomes closer to that predicted by the 1D FDMRC. Without any insulation, the 2D FDMRC model predicts that the radiant system consumes up to 7% more energy use than that predicted by the 1D FDMRC model for a

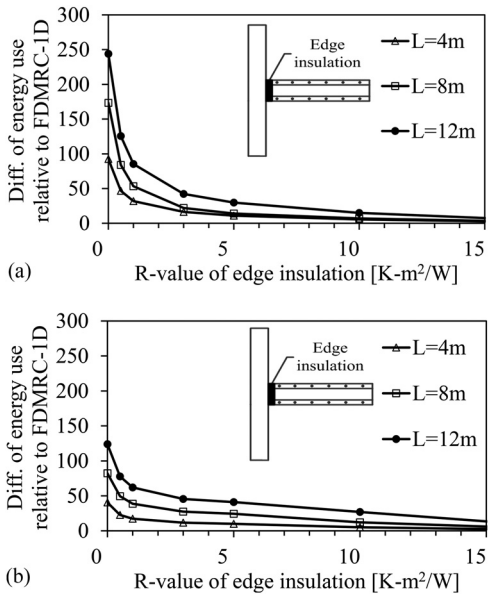

Fig. 10. Impact of R value of insulation at slab-wall joint on radiant system energy consumption with various slab width in Golden, CO: (a) during heating mode; (b) during cooling mode

4-m-wide slab during both heating and cooling modes because of thermal bridge effects. As the insulation is added, the thermal bridging effects are significantly reduced, especially for smaller slabs. In particular, the energy impact associated with thermal bridging effects can be approximately halved during the winter and the cooling seasons with the addition of R-0.5 K m^2/W thermal insulation to the wall-slab joint. Furthermore, Fig. 10 shows that the energy loss

from thermal bridges is significantly increased as the width of the slab is increased. The heating and cooling energy consumption increases for a 4-m slab by 6 and 7%, respectively, when thermal bridging effects are accounted for.

Effect of Insulation Configurations

As discussed previously, the impact associated with thermal bridging effects can be significant for radiant slab systems, especially for small and uninsulated slabs. Thus, it is important to add some insulation to the slab construction to reduce the impact of thermal bridging on energy consumption of radiant systems. The impact of insulation placement on energy performance of the integrated radiant slab systems is assessed by using the 2D FDMRC simulation environment for representative periods during heating and cooling seasons in three U.S. locations: Chicago, IL; Golden, CO; and San Francisco, CA. For the comparative analysis between all the insulation placement configurations, 2.5-cm extruded polystyrene insulation ($R-1$) is being considered for the integrated radiant system. Table 5 indicates the properties of concrete and insulation materials used for the simulation analysis of the two-story building.

Table 5. Properties of Materials Used for Concrete Slab and Thermal Insulation

Material	Conductivity (W/m K)	Density (kg/m^3)	Specific heat (J/kg °C)
Concrete	1.731	2,300	653
Gypsum board	0.160	800	1,090
Mortar	0.930	1,800	1,050
Polystyrene	0.052	24	1214

Fig. 11 illustrates four different insulation configurations considered in the analysis for the effect of insulation placement on the performance of integrated heating and cooling radiant systems, including no insulation (N), horizontal insulation (H), vertical insulation (V), horizontal and edge insulation (H & V).

Fig. 12 compares source energy consumption of an integrated radiant heating and cooling system with various insulation placements. The results clearly indicate that the placement of the insulation has a significant impact on the energy performance of the integrated radiant system for all locations and seasons. During the representative period for the winter season (January 2–4), the vertical insulation decreases the radiant heating energy consumption on average by only 4% compared with the slab with no insulation, regardless of the building location. Meanwhile, horizontal insulation can reduce radiant heating energy consumption by 28%. The most effective insulation configuration for improving the energy efficiency of the integrated radiant heating and cooling system is a combination of horizontal and edge insulation. Indeed, radiant heating energy consumption is reduced by 30% with horizontal and edge insulation during the representative winter period. Similarly, horizontal and edge insulation reduces building energy

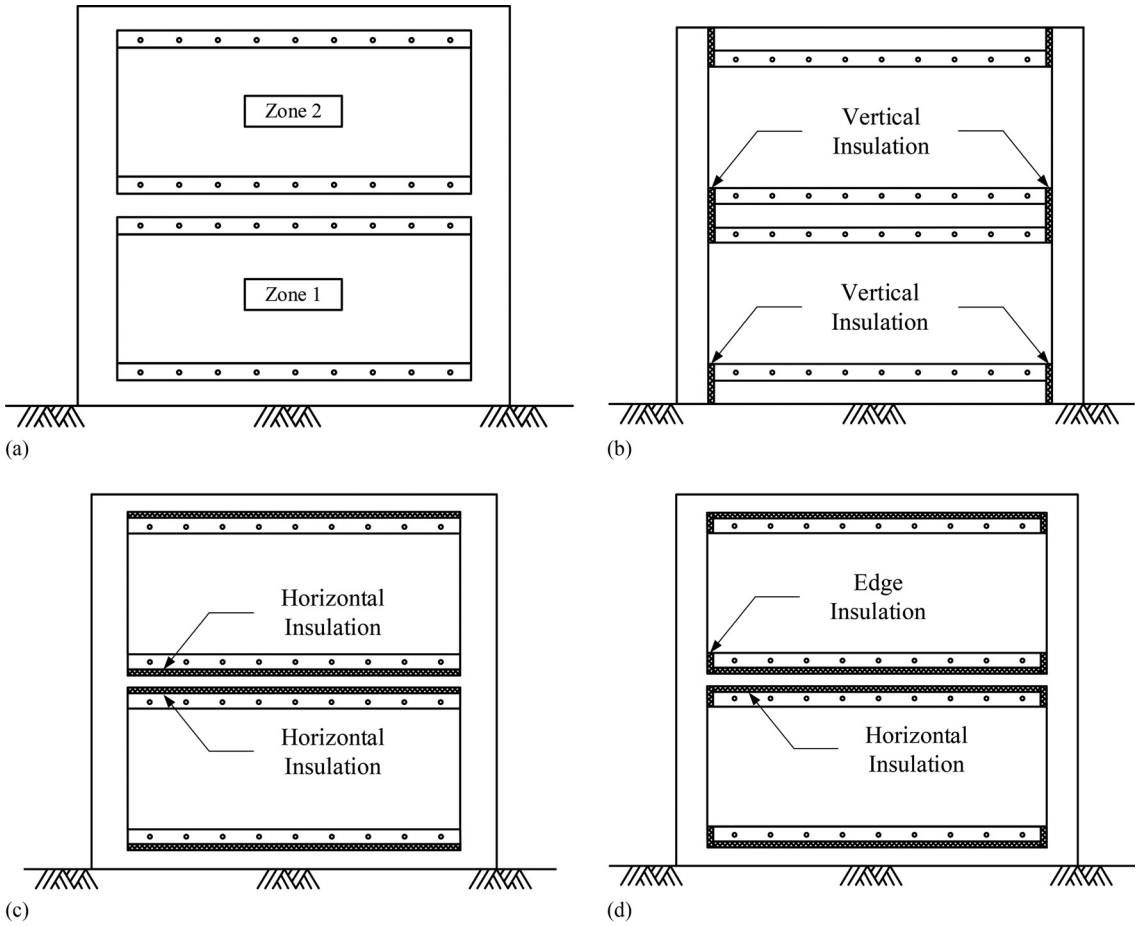

Fig. 11. Insulation placement configurations considered for the integrated radiant heating and cooling system: (a) no insulation; (b) vertical insulation; (c) horizontal insulation; (d) horizontal and edge insulation

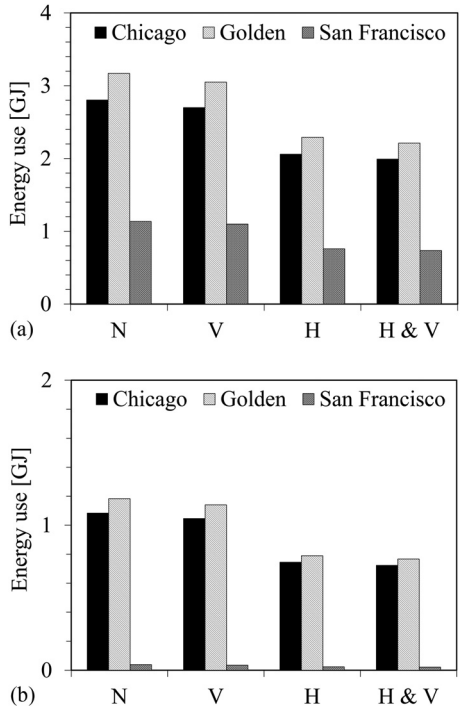

Fig. 12. Comparison of source energy consumption in three U.S. locations by the integrated radiant system for various R-1 insulation placements in the case of 8-m-wide slab: (a) during heating season (January 2–4); (b) during cooling season (August 3–5)

use on average by 35% during the representative cooling period (August 3–5) compared with the case with no insulation. When only horizontal insulation and only vertical insulation is considered, the cooling energy consumption is reduced by approximately 33% and 4%, respectively. Because the floor of the lower zone is in contact with the ground surface and the ceiling of the upper zone is exposed to the outdoor environment, the application of horizontal insulation is more effective than that of the vertical insulation.

Summary and Conclusions

In this paper, a simulation environment is developed for integrated heating and cooling radiant systems for multistory buildings based on a 2D numerical solution for radiant slabs combined with a RC network model for thermal zones. Two main differences can be highlighted between the proposed model described in the manuscript and the current radiant slab model of EnergyPlus:

- First, the developed radiant model in the paper has two heat sources in between vertically adjacent two zones, whereas the traditional radiant floor model has one heat source inside the floor construction. Thus, the proposed radiant model can provide heating/cooling to both upper and lower zones. Currently, EnergyPlus is not capable of modeling this system.
- Second, the radiant system model in EnergyPlus is essentially a 1D model with adiabatic boundary conditions at the edges of the slab with isothermal slab surfaces. The proposed model is based on a 2D heat transfer solution and is able to assess the impact of thermal bridges because of the slab edges.

The predictions from the simulation environment are verified against results obtained from the EnergyPlus simulation for the two-zone building located in Golden, CO, and air-conditioned with an integrated radiant system. Then, the impact of thermal bridging effects on the energy performance of integrated radiant heating and cooling systems are explored using the developed simulation environment tool. Six percent of radiant heating energy consumption can be attributed to thermal bridging effects for the 8-m-wide uninsulated radiant slabs in Golden, CO. Moreover, the radiant cooling system consumes 7% more cooling energy because of thermal bridging when no insulation is used for the 8-m-wide radiant slabs in Golden, CO. It is observed that the relative percentage of energy losses from thermal bridges significantly increases as the width of the slab is reduced. It is estimated that thermal bridges increase heating and cooling energy consumption for a 4-m slab by 7% and 8%, respectively. Based on the verification results, detailed whole-building simulation tools, such as EnergyPlus, ignore the impact of thermal bridges associated with slab-wall joints. In addition, the heat losses through slab-wall joints from the thermal bridge effect can be significantly reduced by adding insulation at the edges of the slab. Specifically, heat losses through the wall-slab joint can be halved with R-0.5 vertical insulation relative to when the integrated radiant slab has no insulation.

The thermal and energy performance of integrated heating and cooling radiant systems is evaluated using the developed simulation environment to assess the impact of insulation placement configurations under various climate conditions. For a representative winter period (January 2–4), horizontal and edge insulation configuration is found to be the most effective for improving the energy efficiency of the integrated radiant heating and cooling systems, regardless of the building location. Indeed, radiant heating energy consumption is reduced by 30% with horizontal and edge insulation during the representative winter period. Similarly, horizontal and edge insulation reduces building energy use on average by 35% during the representative cooling period (August 3–5) compared with no insulation.

Based on the results of the simulation analysis, thermal bridging effects of integrated radiant heating and cooling systems can be significant and should be considered in whole-building simulation analysis to assess the benefits of radiant systems compared with other more conventional air-conditioning systems.

Future Work

In this paper, a stand-alone simulation environment has been developed for radiant slabs with embedded water pipe radiant systems capable of heating or cooling both lower and upper zones of multistory buildings. In the future, the integration of the developed simulation environment within EnergyPlus can be considered; however, the computational efforts associated with obtaining a 2D numerical solution for a radiant slab with its wall joints would increase the simulation time. As an alternative to the full incorporation of the developed 2D radiant slab model, the development of response factors for 2D slabs may reduce the simulation run time. Moreover, future work would adapt the proposed radiant slab model to develop a simulation environment for ventilated slab systems that circulate air instead of water within embedded hollow cores to condition buildings.

Notation

The following symbols are used in this paper:

A = area of the exterior wall (m^2);
c_p = heat capacity (J/kg °C);
$c_{p,c}$ = specific heat of cold water (J/kg °C);
$c_{p,h}$ = specific heat of hot water (J/kg °C);
D = diameter of the embedded pipe (m);
$E_{cooling}$ = radiant cooling energy consumption (J);

$E_{heating}$ = radiant heating energy consumption (J);
E_i = inside surface long-wave radiation;
E_o = outside surface long-wave radiation;
$F_{i,j}$ = view factor;
H = incident radiation;
h_o = convective coefficient at outer surface (W/m^2 K);
h_i = convective coefficient at inner surface (W/m^2 K);
h_w = convective coefficient of the fluid (W/m^2 K);
J = radiosity;
K = thermal conductivity (W/m K);
K_w = thermal conductivity of the fluid (W/m K);
k_{win} = Thermal conductivity of the window;
L = total length of the embedded pipe (m);
$\dot{m}_c$ = chilled water mass flow rate (kg/s);
$\dot{m}_h$ = hot water mass flow rate (kg/s);
Nu = = Nusselt number;
Pr = Prandtl number;
q = generated heating or extracted cooling rate (W/m^3);
q_{CE} = convective parts of internal loads;
$q_{conv,FDM}$ = convective heat transfer rate from the FDM model;
$q_{conv,RC}$ = convective heat transfer rate from the RC thermal network model;
q_{IV} = sensible load caused by infiltration;
Q_{LWR} = long-wave radiation on the outside surface;
Q_{LWX} = long-wave radiation exchange between surrounding surfaces;
Q_{SOLAR} = solar incident on the outside surface;
Q_{SW} = short-wave radiation absorbed by the inside surface;
q_{sys} = heat transfer to/from HVAC system;
$\dot{q}_{TSHG,diffuse}$ = transmitted diffuse solar heat gain [W];
$\dot{q}_{TSHG,direct}$ = transmitted direct solar heat gain [W];
R = thermal resistance of the material (K m^2/W);
Re = Reynolds number;
S_i = absorbed radiation from internal load on the ith face;
T_{out} = outdoor air temperature (°C);
T_s = source location temperature (°C);
$T_{w,in}$ = water inlet temperature (°C);
$T_{w,out}$ = water outlet temperature (°C);
T_{zone} = zone air temperature (°C);
t = time (s);
α = absorptance of solar radiation;
ε = hemispherical emittance of surface;
ε_{win} = emittance of the window surface;
ρ = density ($kg/m^{3)}$; and
σ = Stefan–Boltzmann constant (W/m^2 K^4).

References

DOE-2.1E-053 [Computer software]. Lawrence Berkeley Laboratory, Berkeley, CA.

Arasteh, D., Hokler, C., and Griffith, B. (2010). "Modeling windows in energy plus with simple performance indices." *Technical Rep. LBNL-2804E*, Lawrence Berkeley National Laboratory, Berkeley, CA.

ASHRAE (American Society of Heating, Refrigerating and Air-Conditioning Engineers). (2005). *Handbook of fundamentals*, Atlanta.

ASHRAE (American Society of Heating, Refrigerating and Air-Conditioning Engineers). (2008). *Handbook of systems and equipment*, Atlanta.

Bergman, T. L., Lavine, A. S., Incorpera, F.P., and DeWitt, D. P. (2006). *Fundamentals of heat and mass transfer*, 6th Ed., John Wiley, New York.

Braun, J. E., and Chaturvedi, N. (2002). "An inverse gray-box model for transient building load prediction." *HVAC&R Res.*, 8(1), 73–99.

Çengel, Y. A., Turner, R. H., and Cimbala, J. M. (2001). *Fundamentals of thermal-fluid sciences*, McGraw-Hill, New York.

Conroy, C. L., and Mumma, S. A. (2001). "Ceiling radiant cooling panels as a viable distributed parallel sensible cooling technology integrated with dedicated outdoor air systems/discussion." *ASHRAE Trans.*, 107(1), 578.

DOE (2010). *EnergyPlus Engineering Reference: The reference to EnergyPlus calculations*, Washington, DC.

Fux, S. F., Ashouri, A., Benz, M. J., and Guzzella, L. (2014). "EKF based self-adaptive thermal model for a passive house." *Energy Build.*, 68, 811–817.

Ghatti, V. (2003). "Experimental validation of the EnergyPlus low-temperature radiant simulation." *ASHRAE Trans.*, 109(2), 614–623.

Ho, S. Y., Hayes, R. E., and Wood, R. K. (1995). "Simulation of the dynamic behaviour of a hydronic floor heating system." *Heat Recovery Sys. CHP*, 15(6), 505–519.

Holman, J. P. (1997). *Heat transfer*, McGraw-Hill, New York.

Hottel, H. C., and Sarofim, A. F. (1967). *Radiative transfer*, McGraw-Hill, New York.

Kreith F., and Bohn M. S. (2001). *Principle of heat transfer*, 6th Ed., Cengage Learning, Independence, KY.

Laouadi, A. (2004). "Development of a radiant heating and cooling model for building energy simulation software." *Build. Environ.*, 39(4), 421–431.

Mumma, S. A. (2001). "Ceiling panel cooling systems." *ASHRAE J.*, 43(11), 28–32.

Mumma, S. A. (2002). "Chilled ceilings in parallel with dedicated outdoor air systems: addressing the concerns of condensation, capacity, and cost." *ASHRAE Trans.*, 108(2), 220–231.

Olesen, B. (2008). "Radiant floor cooling systems." *ASHRAE J.*, 50(9), 16–22.

Patankar, S. (1980). *Numerical heat transfer and fluid flow*, CRC Press, Boca Raton, FL.

Seem, J. E. (1987). "Modeling of heat transfer in buildings." Doctoral dissertation, Wisconsin Univ., Madison, WI.

Stetiu, C. (1998). "Radiant cooling in US office buildings: Towards eliminating the perception of climate-imposed barriers." *Rep. No. LBNL-41275*, Lawrence Berkeley National Laboratory, Berkeley, CA.

Strand, R. K., and Pedersen, C. O. (1997). "Implementation of a radiant heating and cooling model into an integrated building energy analysis program." *ASHRAE Trans.*, 103(Pt. 1), 949–958.

Uiuc, L. (2005). *EnergyPlus engineering reference: The reference to EnergyPlus calculations*, U.S. Department of Energy, Washington, DC.

Walton, G. N. (1983). *Thermal analysis research program reference manual*, National Bureau of Standards, U.S. Department of Commerce, Washington, DC.

Wang, S., and Xu, X. (2006). "Parameter estimation of internal thermal mass of building dynamic models using genetic algorithm." *Energy Convers. Manage.*, 47(13), 1927–1941.

Watson, R. D., and Chapman, K. S. (2002). *Radiant heating and cooling handbook*, McGraw-Hill, New York.

Weitzman, P., Kragh, J., Roots, P., and Svendesn, S. (2005). "Modeling floor heating systems using a validated two-dimensional ground-coupled numerical model." *Build. Environ.*, 40, 153–163.

Yazdanian, M., and Klems, J. H. (1994). "Measurement of the exterior convective film coefficient for windows in low-rise buildings." *ASHRAE Trans.*, 100(1), 1087.

Zhang, Z. L. (2001). "Temperature control strategies for radiant floor heating systems." Doctoral dissertation, Concordia Univ., Quebec.